

Research Article

PBMC-derived extracellular vesicles in a smoking-related inflammatory disease model

Nancy E. Gomez¹, Victoria James², Kenton P. Arkill³,
Zubair A. Nizamudeen³, David Onion¹ and Lucy C. Fairclough¹ 

¹ School of Life Sciences, The University of Nottingham, Nottingham, UK

² School of Veterinary Medicine and Science, The University of Nottingham, Nottingham, UK

³ School of Medicine, The University of Nottingham, Nottingham, UK

Extracellular vesicles (EVs) function as mediators of intercellular communication and as such influence the recipient cell function. EVs derived from immune cells can carry out many of the same functions as their parental cells, as they carry costimulatory molecules, antigens, and antigen-MHC complexes. As a result, there is a strong interest in understanding the composition and origin of immune cell-derived EVs in order to understand their role in the pathogenesis of diseases. This study aimed to optimize methodologies to study immune cell-derived EVs. Peripheral blood mononuclear cell-derived small EVs were isolated and observed using conventional transmission electron microscopy and sized by nanoparticle tracking analysis. They were then enumerated and profiled using imaging flow cytometry and were further characterized using a flow cytometric multiplex bead assay. These techniques were then applied to our current research, namely smoking-related inflammatory disease. We present here a comprehensive approach to analyze PBMC-derived small EVs in smoking-related inflammatory disease following the Minimal Information for Studies of Extracellular Vesicle 2018 guidelines.

Keywords: Extracellular vesicles · Exovesicles · Imaging flow cytometry · Spectral flow cytometry



Additional supporting information may be found online in the Supporting Information section at the end of the article.

Introduction

Almost all cell types are known to secrete extracellular vesicles (EVs), membrane-enclosed lipid envelopes that function as mediators of intercellular communication [1]. EVs have the capacity to transfer biological signals and information, including proteins, lipids, nucleic acids, and carbohydrates, between cells and as such influence the recipient cell function [2]. A heterogeneity of EVs has been determined [3]. Based on their biogenesis, EVs are distinguished into two basic types, exosomes and ectosomes.

Exosomes have an endosomal origin and are generated in multivesicular bodies in the form of intraluminal vesicles, and that once formed, the multivesicular body can fuse with the plasma membrane to release its contents as exosomes [3, 4]. The other route of biogenesis is through the release of plasma membrane-derived EVs, known as ectosomes, which include microvesicles [3]. EVs are highly enriched in tetraspanins, particularly CD9, CD63, and CD81, which are commonly used as markers of EVs, although these tetraspanins are not present on every EV [5]. However, the function of tetraspanins extends beyond this, as tetraspanins have been observed to be involved in EV biogenesis, cargo selection, cell targeting, and cell uptake under physiological and pathological conditions [6].

Correspondence: Prof. Lucy C. Fairclough
e-mail: lucy.fairclough@nottingham.ac.uk

Due to their function in cell–cell communication, EVs have been implicated in immune responses associated with numerous diseases [7]. EVs are released by all cells, and immune cells have been shown to release EVs constitutively [8–10]. EVs derived from immune cells can carry out many of the same functions as their parental cells as they carry costimulatory molecules, antigens, and antigen–MHC complexes [10–12]. This allows EVs to transfer antigen presentation ability, directly activate T cells [13, 14], induce maturation and presentation of acquired antigens [15, 16], activate innate immune responses in uninfected macrophages [17], inhibit cytotoxicity of natural killer cells [18], promote apoptosis in T cells and dendritic cells (DCs) [19, 20], and decrease antigen-presentation ability of DCs [7, 9, 20].

The role of EVs in chronic obstructive pulmonary disease (COPD) has become an area of interest as EVs have key cell-to-cell communication roles in cellular responses and are involved in physiological roles and the pathology of various diseases, including pulmonary diseases [21]. Studies have shown that respiratory cells and immune cells release EVs, which can be found in the BALF and can also exit into the circulation [22–24]. Cigarette smoke, a key factor of COPD, may lead to increased release of proinflammatory EVs [22, 23, 25]. The role of EVs in COPD has been systematically reviewed [26] with only a small number of studies focusing on immune cell–derived EVs [27–29]. These studies observed that neutrophils released EVs, which carry neutrophil elastase and contribute to emphysema [28, 29].

The aim of this study was to optimize methodologies to study immune cell–derived EVs following the Minimal Information for Studies of Extracellular Vesicle (MISEV) 2018 guidelines.

Results

In vitro culture platform

We used an in vitro platform that would enable generation, enumeration, and characterization of extracellular vesicles from freshly isolated PBMCs stimulated with anti-CD3/anti-CD28 for 48 hours in culture. To avoid exogenous vesicles, serum-free culture in AIM-V media was chosen. To validate this culture method, cells were stained with markers of apoptosis (Annexin-V) and membrane integrity (PI, Fig. 1A), and it was shown that 72% cells were still viable at 48 h (Fig. 1B).

Analysis of PBMC-derived EVs by conventional transmission electron microscopy and nanoparticle tracking analysis

To confirm the structure and morphology of EVs released from PBMCs, transmission electron microscopy (TEM) was performed. Vesicles were isolated from anti-CD3/anti-CD28 stimulated PBMCs cultured for 48 h by size exclusion chromatography. Isolated vesicles were then examined by TEM. Calcein-stained vesicles were homogeneously spherical, cup-shaped, membrane-

enclosed particles consistent with the morphology of EVs (Fig. 1C). To analyze the size distribution of isolated PBMC-derived EVs, measurements using Nanosight LM10/14 (nanoparticle tracking analysis [NTA]) was performed. The size distribution obtained by NTA showed that most small EVs (sEVs) were under 200 nm in size with a mode of 128 nm (Fig. 1D).

To identify the potential source of vesicles, proteomic analysis of isolated samples was carried out (Supporting information S1). The unique peptides identified in the isolated EV samples were mapped to the relevant proteins. These data were then interrogated to look for protein signatures that have been associated with different vesicle types. Proteins not present in EV samples were listed as not detected. Of the proteins detected, 25 have commonly been reported as associated with EVs [42–44], two proteins usually associated with being part of lysosomes and/or EVs [45], and one protein associated with peroxisomes and/or EVs [46].

Direct in vitro enumeration and characterization of EVs by imaging flow cytometry

Imaging flow cytometry offers high-speed single EV detection, enumeration, and multiparametric characterization, and thus we first optimized staining methods to directly sample PBMC cultures with size exclusion chromatography and profile their whole EV repertoire. To enable sizing of the EVs, reference nanobeads were analyzed (Fig. 1Ei), a gate was then set to include all EVs below the 220 nm nanobeads and were termed as “small EVs” (containing exosomes and smaller microvesicles) (Fig. 1Eii). An exemplar of this gate is shown in a calcein-stained PBMC sample (Fig. 1Eiii). To remove debris and co-incident events, image analysis by “spot counting” was utilized (Fig. 1Fi). Coincident larger particles were removed by gating out any frames containing any visible brightfield spots and only frames containing a single calcein “dot” were selected to remove any coincident or clumped EVs (Fig. 1Fii). Gates were applied to the final plot created that enabled an accurate EV/mL count to be made (Fig. 1Fiii).

Controls

In line with the MISEV 2018 guidelines and the MIFlowCyt-EV framework for standardized reporting of EV flow cytometry experiments, EVs were stained with calcein (Fig. 2Ai) or no calcein (Fig. 2Aii), showing EVs were only present in the gate with calcein-stained samples. A media only control (Fig. 2Aiii) also showed no EVs, and through the addition of Tween-20 detergent to EV samples, it was shown that EV count reduced to 0, indicating the vast majority of material was indeed vesicular in nature (Fig. 2Aiv). This was repeated three times and showed a significant difference in sEVs/mL between the calcein-stained samples and the three controls (Fig. 2B) (one-way ANOVA; $p = 0.0210$). Dunnett’s multiple comparison post hoc analyses showed significant differences between calcein-stained experimental group and no calcein ($p = 0.0233$), media only ($p = 0.230$), and Tween20

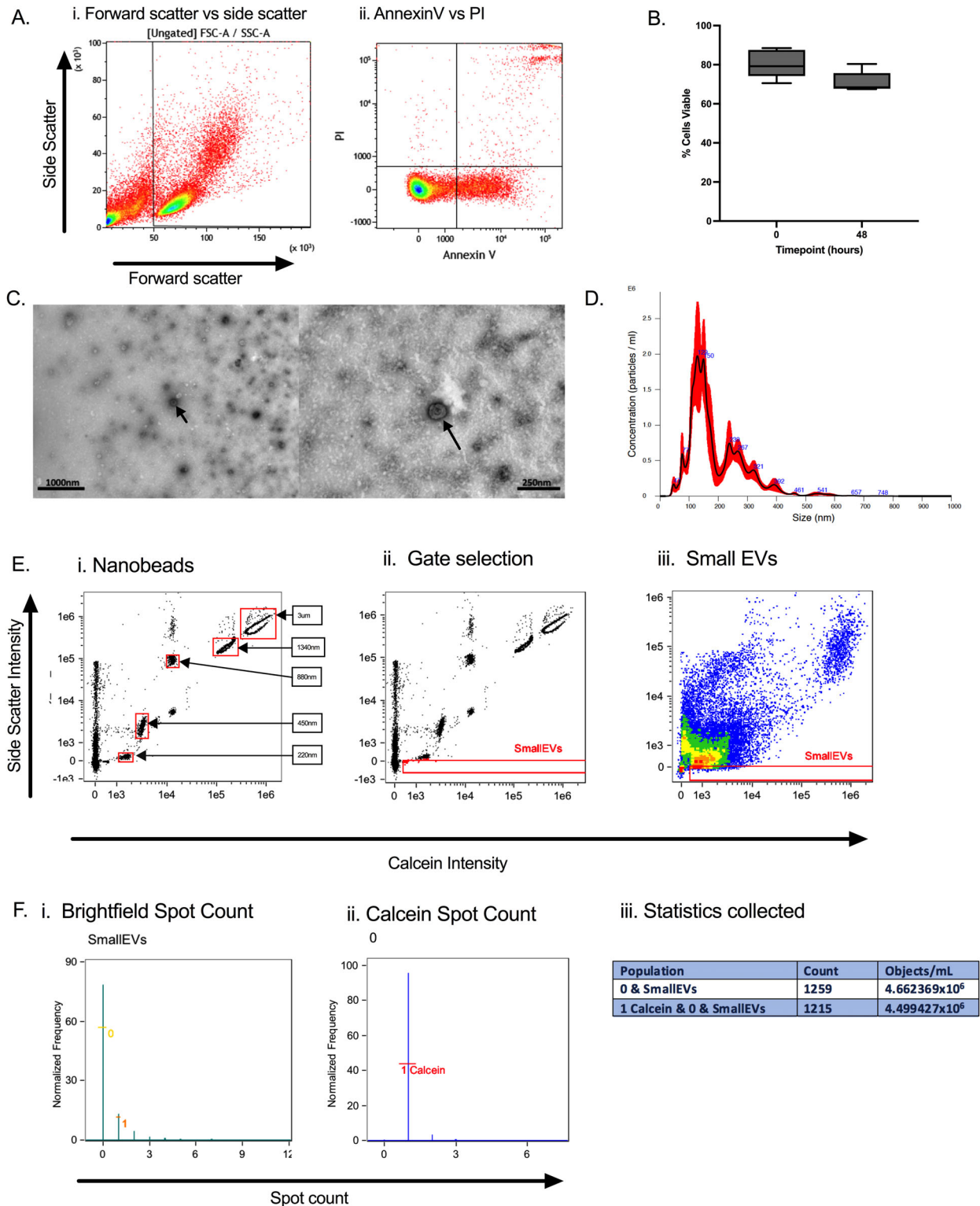


Figure 1. Cell viability by flow cytometry and EV characterization by IFC. (A) Representative density plots of (i) forward scatter versus side scatter to select cells according to their size and granularity, and (ii) annexin V-FITC versus PI analysis of PBMCs. (B) Graph showing percentage cells viable at 0 and 48 h after α -CD3/ α -CD28 activation for five biological repeats. Data are expressed as box and whiskers plot with minimum to maximum values. (C) Exemplar transmission electron micrographs of isolated calcein-stained EVs from PBMCs (11,500–63,100 \times). (D) Size distribution of isolated calcein-stained EV population by NTA for two biological and five technical repeats. (E) Setting gates for small EVs analysis with calcein intensity versus side scatter: (i) nanobeads for reference of size with smallest beads at 220 nm; (ii) small EVs gate created below 220 nm; (iii) small EVs gate copied over to sample collected for further gating. (F) Collecting events of small EVs: (i) spot count get set at 0 for brightfield Channel 09; (ii) spot count for calcein channel 02 set at 1 for single small EVs events; (iii) statistics collected from gated EV population.

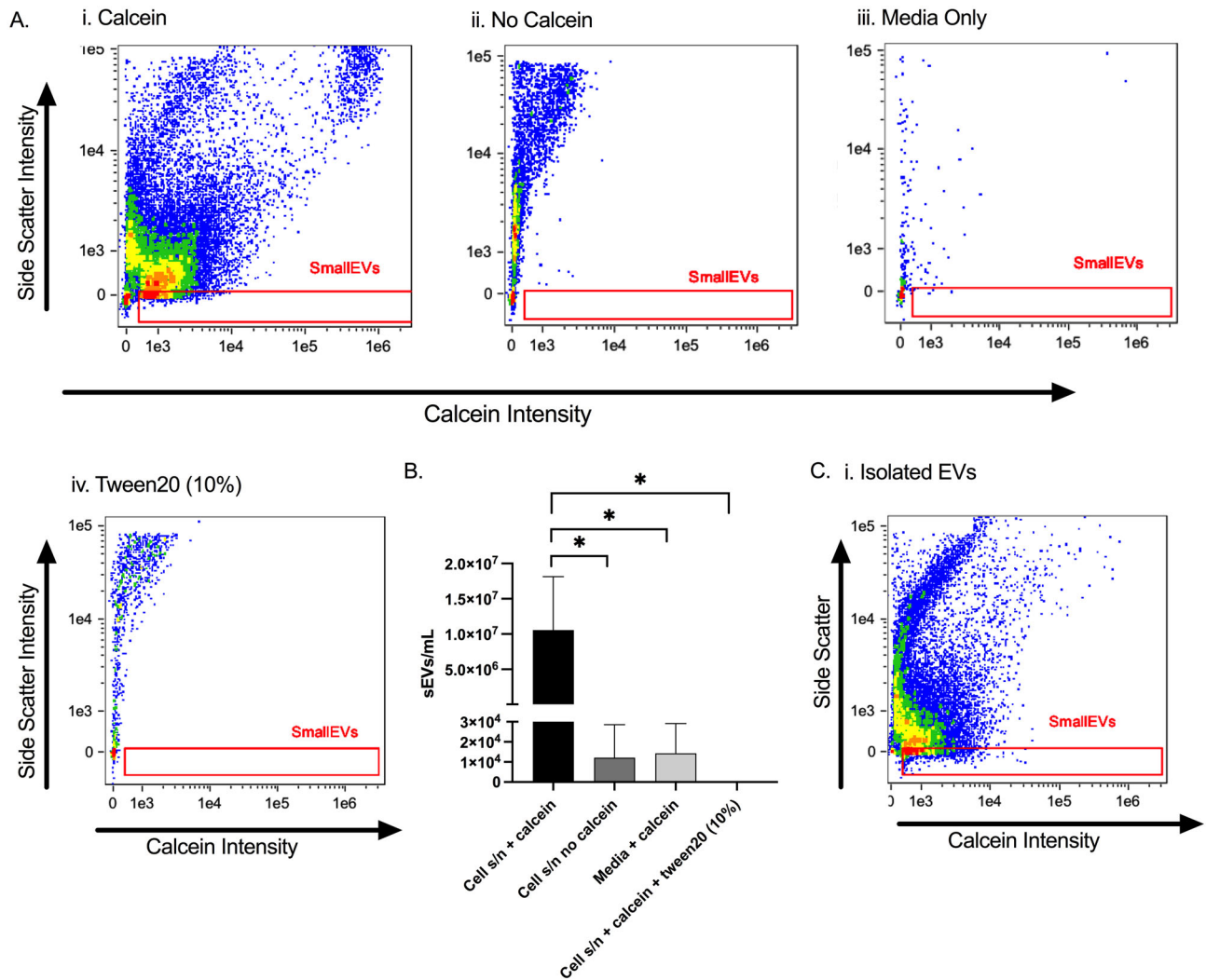


Figure 2. EV characterization and controls for small EV study. (A) Representative images for controls for analysis of EVs: (i) calcein-stained sample; (ii) unstained sample; (iii) calcein-stained AIM-V media only sample; (iv) calcein-stained sample with 10% Tween 20 added. (B) Significantly more sEVs/mL in the calcein-stained sample compared with unstained sample and calcein-stained media only and detergent added samples ($n = 3$ biological repeats). Data are expressed as mean \pm SD. One-way ANOVA, $*p < 0.05$. Dunnett's post hoc analyses indicated that significantly more particles in calcein-stained experimental compared to no calcein ($p = 0.0233$), media only ($p = 0.0230$), and Tween20 ($p = 0.0232$). (C) Isolated calcein-stained sEVs analyzed by IFC.

($p = 0.0232$) groups. As a control, a size exclusion purified EV sample was also analyzed by imaging flow cytometry (IFC), and it was shown that the sEV population fell within the small EV gate utilized for the total PBMC analysis (Fig. 2C).

Characterization of tetraspanin content of EVs

MISEV 2018 guidelines also recommend characterization of EVs by testing for presence of components associated with EVs [31]. Imaging flow cytometry was used to quantify the amount of EV-associated tetraspanins within the calcein-labeled PBMC supernatants. sEVs were gated as before (Fig. 3A) and any out of focus events removed (Fig. 3B) before the application of a sequential set of gates to identify EVs expressing one, two, or three tetraspanins.

The gating strategy to identify tetraspanin expression on EVs is shown (Fig. 3C–E). To set the cut-off for tetraspanin positive EVs, a sample stained only with calcein was analyzed and used to set the gate for CD9, CD63, CD81 positivity (Fig. 3C). Samples stained with calcein and one anti-tetraspanin antibody showed the sEVs to contain CD9, CD63 or CD81 (Fig. 3Di-iii). Labeling EVs with multiple antibodies could possibly lead to reduced sensitivity due to steric hindrance around these small vesicles. We therefore tried staining with two or three simultaneous anti-tetraspanin antibodies in comparison to their single staining. Two tetraspanins (CD81 and CD9) were then plotted against each other to identify double positive EVs (Fig. 3E). The gates were set using fluorescence minus one controls used in conventional flow cytometry. The double positive population was then selected and EVs plotted against the final tetraspanin (CD63) to show EVs that

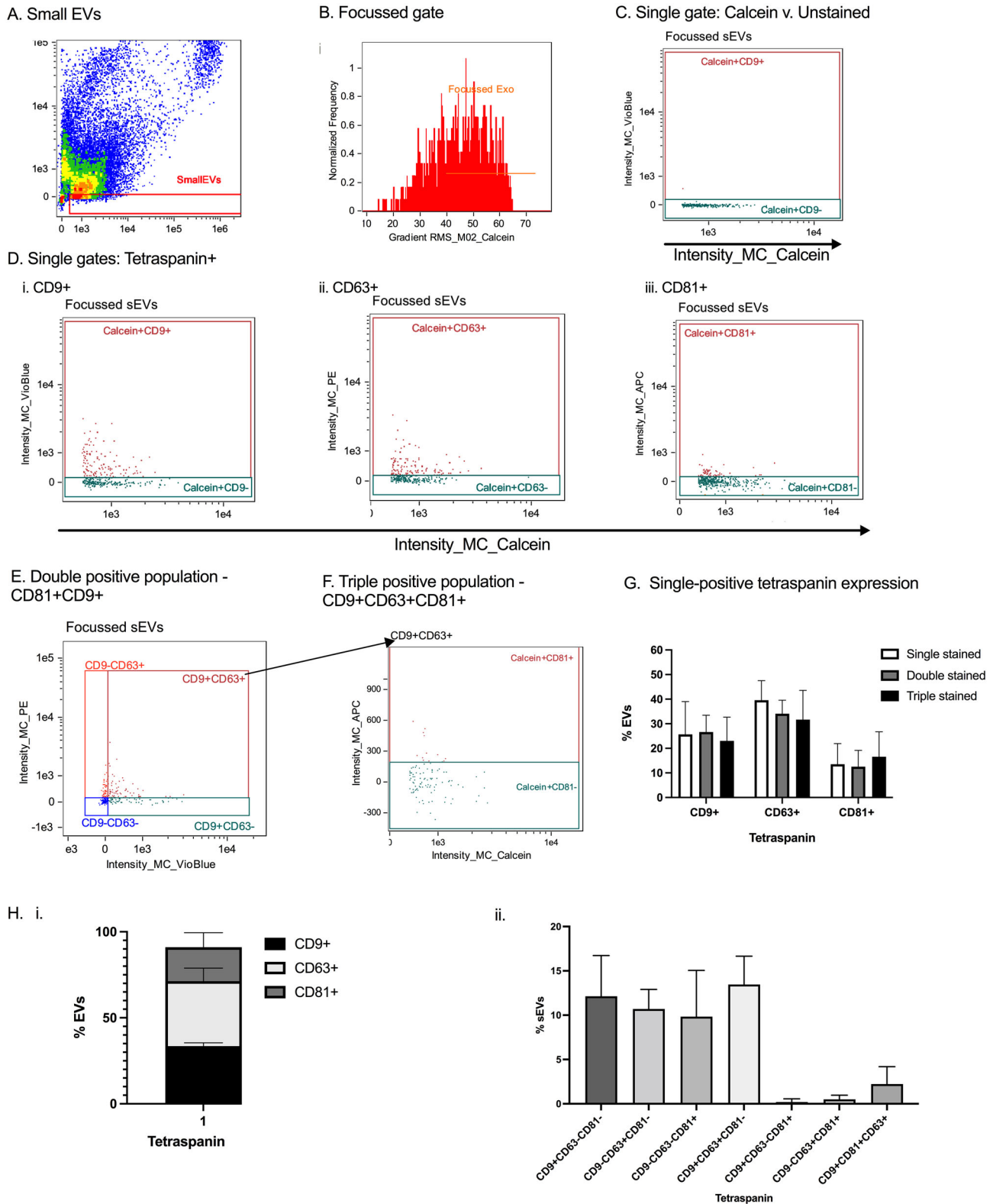


Figure 3. Tetraspanins CD9, CD63, and CD81 in analysis of small EVs by IFC. (A) Small EV gate for small EVs analysis with Calcein intensity versus side scatter. (B) Focused check feature was created using gradient RMS for calcein to remove any artifactual fluorescence when gating tetraspanin data where multiple antibodies were used simultaneously. (C) Representative plot of calcein versus tetraspanins using samples stained with calcein only to create gates for calcein + tetraspanins + sEVs. (D) Representative plots of calcein + tetraspanin + sEVs for (i) CD9; (ii) CD63; (iii) CD81. (E) Representative plots for double tetraspanin+ gates created using samples stained with one tetraspanins only (single colors). (F) Double positive population from E selected for plot gating for triple tetraspanins-positive events. (G) Graph showing over 90% of sEVs express 1 tetraspanin. (H)

were positive for all three tetraspanins (Fig. 3F). We found that even triple staining did not significantly reduce the sensitivity of any of the three markers (Fig. 3G). Triple anti-tetraspanin staining of the calcein labeled PBMC supernatants revealed >90% sEVs to contain at least one tetraspanin on their surface (Fig. 3Hi). In addition, we wanted to profile the percentage of sEVs expressing one tetraspanin (CD9⁺ or CD63⁺ or CD81⁺), those expressing two tetraspanins (i.e., CD9⁺CD63⁺CD81⁻ or CD9⁺CD63⁻CD81⁺ or CD9⁻CD63⁺CD81⁺), and those EVs expressing all three tetraspanins (CD9⁺CD63⁺CD81⁺). Percentage for EVs expressing a single tetraspanin was similar for all three tetraspanins, whereas in the double positive population, the highest percentage was observed for CD9⁺CD63⁺CD81⁻ sEVs, and less than 5% of sEVs expressed all three tetraspanins (Fig. 3Hii).

Surface protein profiling by multiplexed bead assay

In order to further profile the membrane proteins on the EVs and gain insight into lineage-markers, isolated sEVs from unstimulated PMBCs, with more than 70% viability, were phenotyped for 37 surface proteins using the MACSPlex Exosome kit (Fig. 4A). This was done to study EVs that were produced naturally by cells of the immune system. Initial gates were set to select for all 39 capture bead populations (37 surface markers and two isotype controls) by their fluorescence in the FITC versus PE channels (Fig. 4Bi). EVs were quantified on each protein specific population via staining with APC-conjugated detection antibodies. Buffer control and cell assay and are shown in Fig. 4Bii,iii, respectively, where differences of signal intensities of the single bead populations can be observed between the control and the sample. After normalizing the samples, we observed high levels of CD62P, CD41b, CD42a, human leukocyte antigen (HLA)-DRDPDQ, HLA-ABC, CD40, CD69, CD31, and CD29 (Fig. 4C). CD9 and CD63 were observed at higher levels than CD81, in agreement with our IFC data.

Effect of cigarette smoke on EV production by PMBCs

Having optimized and demonstrated novel methods for EV analysis using PMBCs, we then applied these methods to our current research, namely smoking-related inflammatory disease. PMBC culture was exposed to two concentrations of cigarette smoke (1% and 3% cigarette smoke extract [CSE]) or were unstimulated (0% CSE) to determine the effects on PMBC derived EVs. Results show that there were small nonsignificant changes in the number of sEVs produced when exposed to 1% and 3% CSE (Fig. 5Ai) and tetraspanin composition remained unchanged (Fig. 5Aii).

Interestingly, CD9 was most highly expressed regardless of CSE concentration (Fig. 5B). Furthermore, in the double tetraspanin sEV population, CD9⁺CD63⁺CD81⁻ and CD9⁺CD63⁻CD81⁺ sEVs were observed more than CD9⁻CD63⁺CD81⁺ sEVs and less than 10% of sEVs were positive for all three tetraspanins. These results are different to findings of Fig. 3 as previously PMBCs were stimulated with anti-CD3/anti-CD28.

Isolated EVs were then profiled for the surface protein composition using the multiplex bead-based array (Fig. 5C), revealing an altered profile in cigarette exposed derived EVs. Few cell lineage markers were observed. Interestingly, CD40 was significantly downregulated at 1% CSE compared to 3% CSE ($p = 0.0371$). Immune cell markers HLA-ABC (HLA-Class I) and HLA-DRDPDQ (HLA-Class II) were present in the EVs isolated, although their levels did not change on exposure to CSE. Platelet markers, including CD62P, CD41b, and CD42a, were detected at high levels. CD41b was significantly upregulated at 1% CSE compared to control ($p = 0.0295$) and 3% CSE ($p = 0.0222$), and CD42a was significantly upregulated at 1% CSE compared to 3% CSE ($p = 0.0035$). Interestingly, levels of CD69, a marker that shows activation, significantly decreased at 1% CSE compared to 3% CSE ($p = 0.0488$). Furthermore, the adhesion molecule CD31 was significantly downregulated at 1% CSE compared to control ($p < 0.0001$) and 3% CSE ($p = 0.0027$). Control and CSE-EVs displayed similar levels of tetraspanins.

Discussion

This study aimed to optimize techniques to study extracellular vesicles produced by immune cells. PMBC-derived sEVs were first observed by TEM and NTA, showing presence of EVs using well-established EV techniques. sEVs were then enumerated and profiled using imaging flow cytometry and further characterized using a multiplex bead assay and spectral flow cytometry. These two techniques have the advantage over conventional TEM and NTA through their ability to detect high numbers of EVs.

In this study, we show the use of calcein AM to enumerate sEVs using flow cytometry. The use of IFC for EV analysis allows us to overcome some of the challenges of measuring EVs in the submicrometer range often encountered with traditional flow cytometry, such as coincidence detection. The IFC has a precision syringe-based sample acquisition that allows for accurate enumeration of EV concentrations without using counting beads [47]. Calcein AM also allows for discrimination between intact EVs and debris, as it requires hydrolysis by intravesicular esterase to be converted into a fluorescent analogue that is EV impermeant, and has been used to successfully stain for EVs [33–35, 48]. A study by Gray et al. [33] has shown that calcein AM was as sensitive at detecting EVs

Graphs showing (i) no significant differences on the ability to detect CD9, CD63, or CD81 positive sEVs with addition of multiple antibodies. Data are expressed as mean \pm SD. Two-way ANOVA; Tukey's multiple comparisons post hoc analyses indicated no significant differences observed. (ii) Percentage of sEVs expressing individual tetraspanin only (CD9⁺ or CD63⁺ or CD81⁺), expressing two tetraspanins (i.e. CD9⁺CD63⁺CD81⁻ or CD9⁺CD63⁻CD81⁺ or CD9⁻CD63⁺CD81⁺) and expressing all three tetraspanins (CD9⁺CD63⁺CD81⁺). Percentage was determined from triple-tetraspanin and calcein-stained samples (G-H = 5 biological repeats).

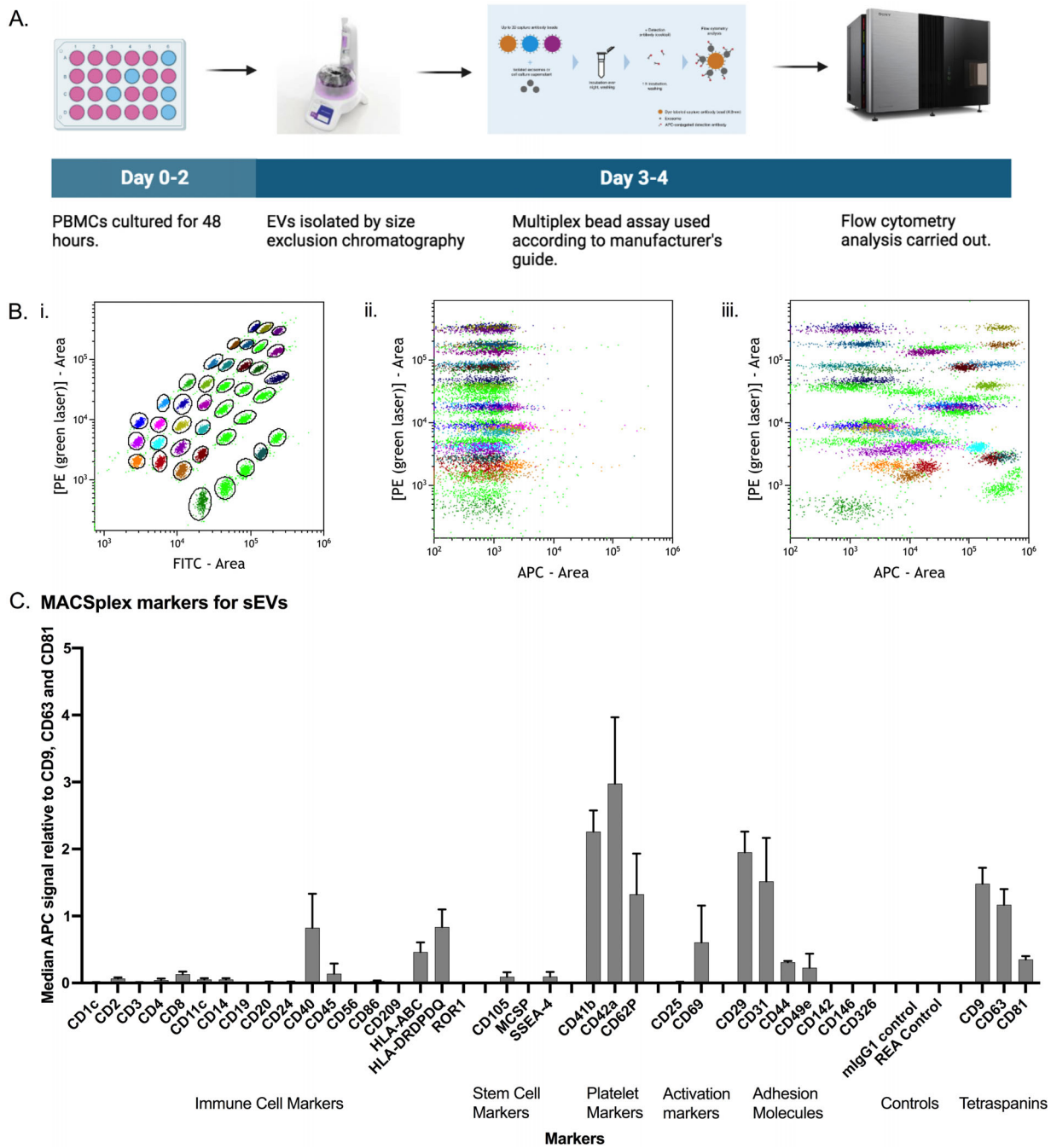


Figure 4. Multiplex bead-based platform to analyze markers on surface of sEVs. (A) Workflow of methodology. PBMCs were cultured to generate sEVs. sEVs were isolated by size exclusion chromatography and incubated overnight with 39 different bead populations coupled with capture antibodies. sEVs bound to beads were detected with a cocktail of anti-CD9-APC, anti-CD63-APC, and anti-CD81-APC antibodies. (B) Representative images of (i) 39 bead populations identified by their fluorescence in the FITC vs PE channel; (ii) APC versus PE signal intensities of single bead populations in buffer control; (iii) APC versus PE signal intensities of single bead populations in stimulated assay. (C) Quantification of the median APC fluorescence values for all bead populations after background correction and relative to CD9, CD63, and CD81 ($n = 3$ biological repeats).

as PKH26 and selectively labeled intact EVs. As the staining was applied to both purified EVs and culture supernatant in this study, it was of particular importance to selectively stain intact EVs as culture supernatants are more likely to contain variable numbers of disrupted EVs and EV fragments. Furthermore, techniques such as NTA and other methods used for EV detection are unable to dif-

ferentiate heterogeneous EVs from other particles with overlapping size, including lipoproteins and aggregated protein particles [5]. A previous study showed that calcein AM had low sensitivity in EV samples, however, EVs were isolated prior to being stained with calcein AM [48]. In this study, samples were stained in culture and analyzed by IFC, with a gating strategy that allowed selection of

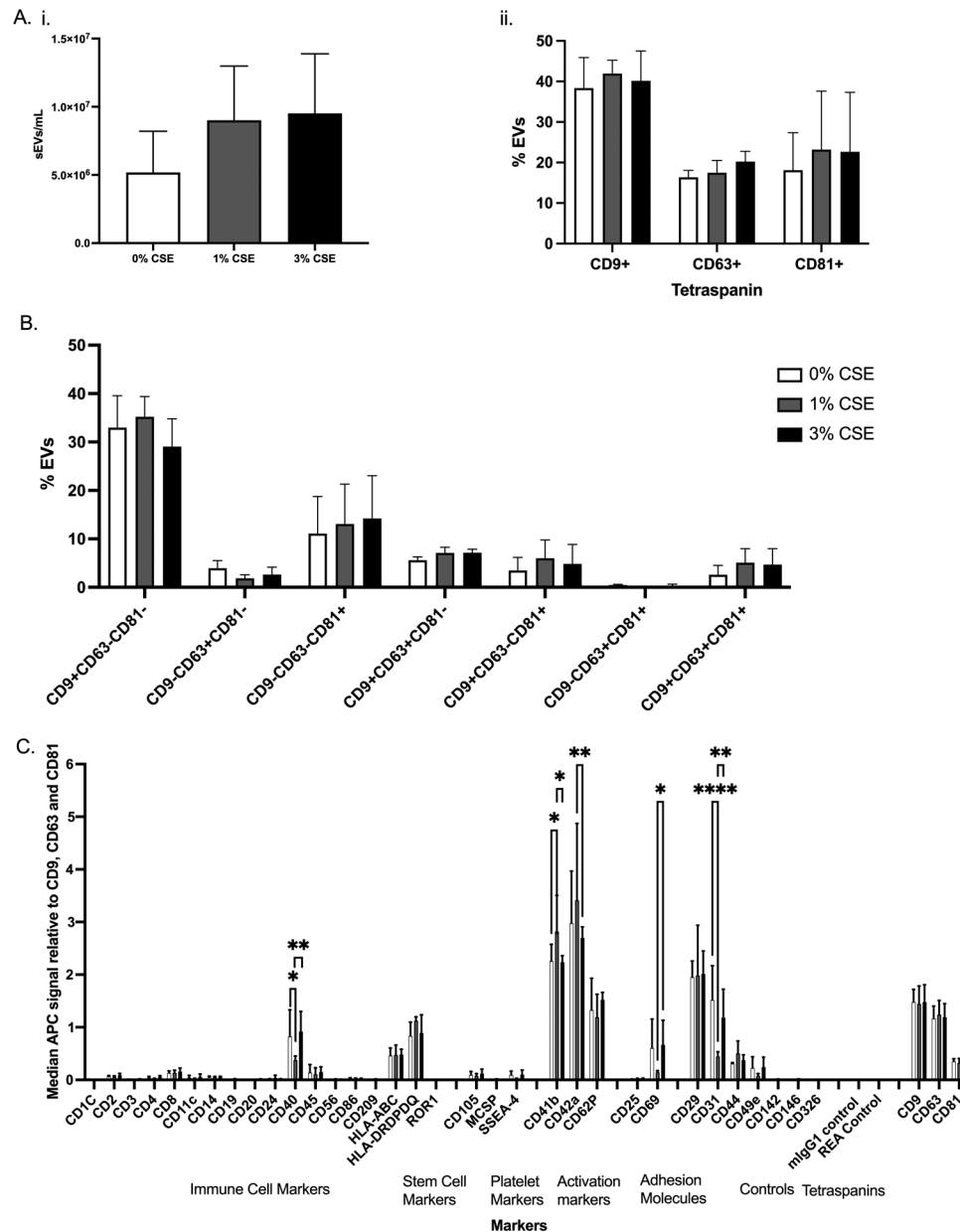


Figure 5. Characterization of small EVs derived from CSE-stimulated PBMCs (A–C = 3 biological repeats). (A) IFC data collected for control and CSE-stimulated samples: (i) sEVs/mL data of control and CSE samples. Data are expressed as mean ± SD; One-way ANOVA; Tukey's multiple comparisons post hoc analyses indicated no significant differences observed. (ii) Percentage of sEVs positive for each tetraspanin (CD9, CD63, CD81) for control and CSE-stimulated samples. (B) Percentage of sEVs expressing individual tetraspanin only (CD9⁺ or CD63⁺ or CD81⁺), expressing two tetraspanins (i.e. CD9⁺CD63⁺CD81⁻ or CD9⁺CD63⁻CD81⁺ or CD9⁻CD63⁺CD81⁺) and expressing all three tetraspanins (CD9⁺CD63⁺CD81⁺) for control and CSE-stimulated samples. Data are expressed as mean ± SD; two-way ANOVA; Tukey's multiple comparisons post hoc analyses indicated no significant differences observed. (C) Surface marker profiles of control and CSE-sEVs. Expression of CD41b was significantly upregulated for 1% CSE-EVs compared to control ($p = 0.0295$) and 3% CSE-EVs ($p = 0.0222$). Expression level of CD42a was significantly increased between 1% CSE-EVs and 3% CSE-EVs ($p = 0.0035$). Expression levels of CD40 ($p = 0.0371$) and CD69 ($p = 0.0488$) were significantly lower between 1% CSE and 3% CSE EVs. Expression levels of CD31 was significantly lower at 1% CSE compared to control ($p < 0.0001$) and 3% CSE ($p = 0.0027$). Data are expressed as mean ± SD; two-way ANOVA; Tukey's multiple comparisons post hoc analyses.

small EVs (i.e., under 200 nm). Isolated EVs were also analyzed by TEM and NTA to confirm observed sEV population. Size distribution of isolated EVs observed by NTA showed most EVs were under 200 nm in size with a mode of 128.4 nm, in agreement with the data generated by TEM. Isolated EVs were analyzed by IFC to

demonstrate that the EV population could still be identified with the gating strategy developed for sEVs.

To further profile sEVs, this study observed the presence of tetraspanins (namely, CD9, CD63, and CD81), which have broad tissue expression and as plasma membrane and endosome

membrane proteins can be used as specific EV markers. The use of tetraspanins is an additional tool to overcome limitations of EV detection [5]. Additionally, tetraspanins characterization of EVs could indicate the subcellular origin of EVs, allowing for determination of the exosomal or ectosomal nature of EVs [49]. Previous studies have analyzed co-expression of two tetraspanins using flow cytometry [50, 51]; however, co-expression of all three tetraspanins has not been assessed using IFC. CD9-CD63-CD81-triple-positive EVs have been previously observed to comprise a substantial portion of EVs using total internal-reflection microscopy [52]. In this study, we detect three different tetraspanins per sample with the use of IFC to analyze subsets of EVs. Here, we show that presence of all three tetraspanins can be simultaneously detected along with calcein without compromising the sensitivity of staining. We also demonstrate higher numbers of sEVs expressing both CD9 and CD63 than sEVs bearing CD63 and CD81 or CD9 and CD81. These data are in keeping with those previously reported for EVs isolated from blood samples, where CD81⁺ EVs form the smallest EV subpopulation [53]. Furthermore, results show over 90% of sEVs expressed one tetraspanin on their membrane. Less than 10% of sEVs did not have any of the three tetraspanins, demonstrating selective labeling with CD9, CD63, and CD81 leaves some sEVs uncharacterized. Tetraspanins found in EVs have been shown to function in EV biogenesis, cargo selection, cell targeting, and cell uptake under physiological and pathological conditions [54]. CD9 and CD81, along with integrin $\alpha_v\beta_3$, have been suggested to be involved in the targeting and uptake of EVs by DCs [6].

To further profile the membrane of sEVs for lineage-specific proteins, isolated sEVs from PMBCs were phenotyped for 37 surface markers using the MACSplex Exosome kit. Here, we show the presence of nine surface proteins (CD62P, CD41b, CD42a, HLA-DRDPDQ, HLA-ABC, CD40, CD69, CD31, and CD29) at high levels. These EVs carried molecules that are involved in immune regulation (HLA-DRDPDQ, HLA-ABC, and CD40) and cell adhesion (CD31 and CD29). Furthermore, CD62P, CD41b, and CD42a are markers expressed on platelets and megakaryocytes [55], suggesting EVs derived from these sources. This reflects the fact that platelet- and megakaryocyte-derived EVs are the most abundant EVs in human blood, accounting for more than half of all EVs in the peripheral blood [56, 57].

In this study, we then examined the effects of CSE on sEVs released from PMBCs, observing the concentration and membrane profile of sEVs. The concentrations of CSE (1% and 3%) used in this study were based on those used in previous studies observing the effect of CSE on cells *in vitro* [37–39] and based on a previous study of a “physiological” *in vitro* model to analyze cellular and histological effects of cigarette smoke in culture [58]. We did not observe any significant differences in the number of sEVs from control or CSE-exposed PMBCs. A previous study has reported significantly more EVs released from CSE-exposed primary human DCs (iDCs) [59], although CSE concentration for that study was markedly higher at 50%, which is beyond physiological range. In this study, we used CSE concentrations of 1% and 3%, consistent with previous studies of the effects of CSE on cells

in vitro [37–41]. Furthermore, observation of tetraspanin expression in this study showed that tetraspanin composition remained unchanged after exposure to CSE. CD9 was the highest expressed tetraspanins, followed by CD81, with CD63 being the tetraspanin least expressed. Additionally, sEVs expressing both CD9 and CD63 or CD9 and CD81 were most highly detected, whereas sEVs bearing CD63 and CD81 were minimally detected. About 5% of sEVs were shown to bear all three tetraspanins. Differences in the expression of tetraspanins can be due to differences in the activation state of the cells producing EVs, as upon stimulation cells undergo phenotypic changes depending on the particular stimulus given to the cells [60]. Studies have shown that immune-cell derived EVs are functionally active as they harbor a range of immune cell-derived surface receptors and effector molecules from parental cells [8, 61]. As a result, immune cell-derived EVs can modulate specific mechanisms of the innate and adaptive immune response. Therefore, we examined the expression of 37 exosomal surface markers in sEVs isolated from PMBCs exposed to CSE at different percentages, reflecting membrane proteins of the original cells. Data from the MACSplex assay show significant differences in expression of CD40, CD41b, CD42a, CD69, and CD31 between control and CSE or between CSE concentrations. CD40 is a costimulatory molecule expressed by B cells, professional APCs (including macrophages/monocytes, and DCs), sometimes T cells, as well as nonimmune cells and tumors [62–64]. CD40-CD40L coupling is important in various aspects of the immune response, including activation of kinases, expression of genes related to cellular stress, regulation of apoptosis, expression of surface molecules, as well as activation and differentiation of immune cells and autoimmunity [63, 65, 66]. Cigarette smoke has been shown to increase CD40 expression on lung mononuclear cells of mice exposed to cigarette smoke for 4 weeks and on BM-derived DCs from healthy mice cultured *in vitro* with CSE for 24 h [67]. Another study demonstrated an initial increase in CD40 expression in primary murine DCs cultured *in vitro* with CSE for 24 h; however, this expression was significantly down-regulated after continuous CSE exposure [68]. Here, exposing human PMBCs to CSE *in vitro* for up to 48 h, we show significantly decreased levels of CD40 detected at 1% CSE, suggesting that timing of exposure may also affect expression of CD40 observed. Additionally, in this study, we show significant increased expression of CD41b and CD42a at 1% CSE. CD41b and CD42a are markers of platelets, suggesting these are platelet-derived EVs [57, 69]; however, currently there is no research in platelet-derived EVs and smoking. CD69 is detected on the surface of activated lymphocytes as an early lymphocyte activation marker [55]. CSE has previously been shown to significantly inhibit the expression of CD69 by natural killer cells [70, 71]. However, cell surface expression of CD69 on cytotoxic T cells was enhanced in COPD and smokers with normal lung function compared to never-smokers [72]. In this study, we showed decrease of CD69 expression on sEVs at 1% CSE, suggesting reduced activation of cells producing EVs after exposure to 1% CSE. Furthermore, CD31 is an endothelial cell adhesion molecule expressed by vascular endothelial cells platelets and leukocytes [73, 74] and is thought

to have a function in downregulating T-cell activation [74, 75]. In this study, EV expression of CD31 decreased at 1% CSE concentration compared to control and 3% CSE concentration. Contradicting studies have shown increased CD31 expression in EVs derived from primary human DCs exposed to 50% CSE [59] and increased CD31⁺ EMPs in circulation in rats after exposure to cigarette smoke [26, 76]. Here, we also observed expression of HLA-ABC (MHC-I) and HLA-DRDPDQ (MHC-II), although there were no significant differences in level of expression between concentrations of CSE and control for both markers. Previous study has shown increased expression of HLA-ABC in EVs derived from primary human DCs exposed to 50% CSE [59]. Another study observed significantly lower expression of HLA-ABC and HLA-DRDPDQ in bronchoalveolar lavage-derived macrophages from smokers; however, the study also exposed alveolar macrophages from healthy volunteers to 10% CSE in vitro and observed no significant differences in expression of HLA-ABC or HLA-DRDPDQ [77]. HLA-ABC is fundamental for the activation of cytotoxic CD8⁺ T lymphocytes and can be found on the surface of almost all nucleated cells [78, 79]. HLA-DRDPDQ molecules are classically found only on B cells and APCs, such as DCs and macrophages, thus having the ability to activate CD4⁺ T cells [78]. Furthermore, there were no significant differences in the expression of tetraspanins CD9, CD63 and CD81 between control and CSE-stimulated EVs. Overall, studies have shown that cigarette smoking alters the membrane profile of EVs in humans and this could be due to CSE exposure altering signaling pathways that affect EV formation and/or release [59, 80, 81], in agreement with the study presented here.

In conclusion, we have outlined a protocol to analyze immune cell-derived EVs. This protocol focuses on high-throughput flow-based methods, including IFC that incorporates a novel gating strategy (using the spot count feature) and a rapid staining protocol that allows for quantification of EVs in culture and following isolation. Additionally, we have demonstrated the ability to observe three tetraspanins on calcein-labeled sEVs by IFC. Furthermore, we have used spectral flow cytometry to profile the membrane protein composition of sEVs for lineage-specific proteins.

Materials and methods

processing of blood samples and PBMC isolation

Ethical approval was obtained from the University of Nottingham Medical School Ethics committee (FMHS REC ref121-1706) and individuals consented to the study prior to blood donation. In total, five healthy volunteers (three females, two males) between the ages of 20–25 were recruited to this study. Blood was drawn by venepuncture and collected into heparin tubes for PBMC isolation. Isolation of PBMCs from fresh whole blood was done by histopaque density gradient centrifugation in serum-free AIM-V medium (ThermoFisher). Specifically, 20 mL of blood

Table 1. Assay controls to enable accurate extracellular vesicles analysis and reporting.

Assay controls	Details
Procedural controls	AnnexinV/PI staining of PBMCs producing EVs
Buffer only	AIM-V medium only with no stimulators; calcein AM added
Buffer with reagents	AIM-V medium only with stimulators; calcein AM added
Unstained controls	No calcein AM, no fluorophore-associated monoclonal antibodies
Isotype controls	Isotypes for anti-tetraspanins monoclonal antibodies; calcein AM added
Single-stained controls	Calcein AM only; Calcein AM with single tetraspanin
Detergent treated EV samples	10% Tween20 added; calcein AM added

was diluted 2:1 in AIM-V medium. The diluted blood was layered over histopaque (Sigma, Poole, UK) and centrifuged at 800 g for 22 min, with an increase speed of 1 and a decrease of 0. The resultant mononuclear layer was removed from the surface of the histopaque and washed twice with AIM-V medium, then re-suspended in a known volume. A cell count was performed using a haemocytometer, and PBMCs were resuspended at 2×10^6 cells/mL in AIM-V medium.

T-cell activation

Human PBMCs were stimulated with immobilized anti-human CD3 and soluble anti-human CD28 antibody (at a final concentration of 2 μ g/mL). Briefly, 2 μ g/mL anti-CD3 (diluted in sterile PBS) [30] was added to wells in a 96-well cell culture plate (Corning, Flintshire, UK; Ref. 3799) and incubated (37°C, 5% CO₂) for 90 min. The plate was then washed twice with cold sterile PBS. PBMCs were added at a final concentration of 2×10^6 cells/mL, and 2 μ g/mL anti-CD28 was added. Stimulated PBMCs were cultured for up to 48 h.

Assay controls for EV analysis

Following MISEV guidelines and the MIFlowCyt-EV framework for standardized reporting of EV flow cytometry experiments, Table 1 shows the controls used to enable accurate analysis of EVs [31, 32].

Cell viability (annexin V and PI staining)

Cell viability and apoptosis of PBMCs was tested during time of EV collection using annexin V/PI staining. Note that 10^6 cells

were stained with annexin/PI using the Annexin V-FITC kit (Miltenyi Biotec, Woking, UK), according to manufacturer's instructions. Flow cytometric analysis of cells labeled was performed using BD FACS Canto A (BD Biosciences). A minimum of 20,000 events were acquired. Data were analyzed with the use of Kaluza Software (Beckman Coulter V2.0).

EV staining using calcein AM and anti-tetraspanin monoclonal antibodies

Calcein AM staining for EVs was carried out for EV analysis using IFC. Previous studies have reported successful labeling of EVs using calcein AM [33–35], and this method has been used to distinguish between intact EVs and debris. A 1 mM stock solution of calcein AM (Biolegend) was prepared by reconstituting in anhydrous DMSO and added to cell suspensions with a final concentration of 0.1 μ M and incubated for 1 h (37°C, 5% CO₂).

For staining, 1 μ L of anti-tetraspanin monoclonal antibody (CD9-VioBlue (130-118-809), CD63-PE (130-118-077), and CD81-APC (130-119-787) (Miltenyi Biotec)) was added per test conducted. Samples were incubated at 37°C for 30 min. Equivalent concentrations of the respective isotype controls were added to samples to determine the degree of nonspecific binding. In addition, validation of vesicle detection was determined by labeling of samples that had been treated with 10% Tween20 (10 μ L) at room temperature for 15 min.

EV isolation by size exclusion chromatography

Note that 4 million cells (2 million cells/mL) were cultured for 48 h. Supernatants were removed from wells and concentrated to approximately 400–500 μ L using a Vivaspin 20, 10 kDa ultrafiltration unit (Sartorius) by centrifuge at 3000 \times g for 10 min to pre-clear cell culture supernatant. EVs were then isolated by size exclusion chromatography using qEV original 35 columns with an automatic fraction collector (Izon Science) that collects EVs ranging from 35 to 350 nm. Fractions 1–5 of 1.0 mL were collected and concentrated using Vivaspin 20 column at 3000 \times g for 10 min. EV fractions (~500 μ L) were transferred into 1.5-mL microcentrifuge tubes covered with film to prevent drying and then stored at –80°C.

As with other EV isolation protocols, the complete elimination of potential cell contamination cannot be confirmed. Proteomic analysis of isolated samples was thus carried out to examine vesicle types present in the samples as identified by protein markers (Supporting information S1).

Transmission electron microscopy

Isolated EVs were fixed in 3% glutaraldehyde solution in cacodylate buffer for 30 min. Note that 10 μ L of sample was added

to poly-L-lysine treated carbon film slot grids (EM resolutions) and left to settle for 15 min. Samples were then washed twice with ddH₂O and stained with 1% uranyl acetate for 5 min, and the excess amount was removed using blotting paper. TEM was carried out using a Tecnai Biotwin-12 with an accelerating voltage of 100 kV.

Nanoparticle tracking analysis

EVs for NTA analysis were isolated by size exclusion chromatography as stated above. An LM10/14 Nanosight (Nanosight, Malvern Panalytical) instrument was used to analyze isolated EVs. Prior to analysis, a 1:10 dilution of 100 nm carboxylated polystyrene (CPC100; IZON) and a 1:1000 dilution of 200 nm polystyrene (Malvern Panalytical) nanoparticles were used to test the sensitivity of the instrument [36]. EV samples were diluted such that less than 200 particles were tracked per image. Automatic settings were applied for the minimum expected particle size, minimum track length, and blur settings. For capture settings, screen gain was set at 1, and camera level was set at 13 (shutter 1390; gain 372). For analysis settings, screen gain was set at 13, and the detection threshold was set at 3. Five 60 s movies were captured at 30 frames per second for each sample. Data processing and analysis of particle size distribution were performed using NTA Software 3.3 Dev build 3.3.301 (Malvern Panalytical).

Imaging flow cytometry

IFC was performed using ImageStreamX MKII (Luminex) with the following laser powers: 405 nm (120 mW), 488 nm (200 mW), 561 nm (200 mW), 642 nm (150 mW) and side scatter (SSC). Channels 01 and 09 were set to brightfield (BF) and channel 12 was set to side scatter (SSC). Samples were acquired, for a time span of 10 min unless the acquisition was complete, using the software INSPIRE. Reference nanobeads (NFPPS-52-4K) (Spherotech) were analyzed to display a reference standard. Data analysis was performed using IDEAS software. IDEAS feature “objects/mL” was utilized to determine the concentration of gated small EVs. A spot count feature was first created (Spot Count_Spot (M09, Ch09, Bright, 1, 1, 1)_4) to exclude any events with a brightfield image. A second spot count feature (M02, Calcein, Bright, 1, 5, 1)_4 was created to include only events with a single calcein “dot” and to exclude any coincident or clumped EVs.

Protein measurements

Protein concentrations in isolated EV fractions were measured using a BCA protein assay kit (ThermoFisher) according to manufacturer's instructions.

MACSplex surface protein profiling using spectral flow cytometry

The MACSplex Exosome Kit (Miltenyi Biotec) allows for detection of 37 surface markers present on EVs plus two isotypes. These include CD3, CD4, CD19, CD8, HLA-DRDPDQ, CD56, CD105, CD2, CD1c, CD25, CD49e, ROR1, CD209, CD9, SSEA4, HLA-ABC, CD63, CD40, CD62E, CD11c, CD81, MCSP1, CD146, CD41b, CD42a, CD24, CD86, CD44, CD326, CD133/1, CD29, CD69, CD142, CD45, CD31, CD20, CD14, REA, and IgG1. The MACSplex kit was used according to the manufacturer's instructions for the assay using 1.5-mL tubes. Samples were analyzed using an ID7000 flow cytometer (Sony Biotechnology) and data analyzed using Kaluza (Beckman Coulter V2.0). For analysis, the median fluorescence intensity (MFI) for all 39 capture bead subsets were background corrected by subtracting respective MFI values from matched non-EV buffer or media controls treated like EV-containing samples (buffer/medium + capture beads + antibodies). Data normalization was directed toward CD9/CD63/CD81 APC signal by using the mean of the median signal intensity of the MACSplex Exosome Capture Beads CD9, CD63, and CD81 as the normalization factor for each sample. The signal intensity of all beads was divided by the normalization factor of the respective sample.

Cigarette smoke extraction

To generate a model system to assess the methodologies developed, CSE was used. CSE is an aqueous solution containing many of the chemicals associated with the exposure to cigarette smoke. The solution was made fresh on the day of the experiment. The smoke generated from combustion of a Marlboro Red cigarette was bubbled slowly through phenol red-free RPMI medium (Sigma) in a 25-mL Universal tube to obtain the CSE. The CSE was then filtered using a 0.45 μ m filter. A dilution series of CSE was prepared and the absorbance was measured using Nanodrop ND-1000 spectrophotometer at 320 nm. The dilution required to get an absorbance of 0.15 (100% CSE) was then calculated. A concentration range of 1–3% CSE was used to treat PBMCs, consistent with previous studies of the effects of CSE on cells in vitro [37–41].

Data and statistical analysis

Data analysis was performed using Prism software, version 8.2.1c (GraphPad). Statistically significant differences of sEV concentration for sample versus controls were analyzed by ordinary one-way ANOVA, followed by Dunnett's multiple comparisons test. Statistically significant differences of percentage focused single-versus double- versus triple-stained sEVs for each tetraspanin (CD9, CD63, CD81) were analyzed by two-way ANOVA, followed by Tukey's multiple comparisons test. Statistically significant differences of sEV concentration for control versus CSE-exposed

PBMCs and 1% versus 3% CSE-exposed PBMCs were assessed with ordinary one-way ANOVA, followed by Tukey's multiple comparisons test. Statistical significance of differences in percentage focused sEVs was assessed with two-way ANOVA, followed by Tukey's multiple comparisons test for each tetraspanin at each CSE concentration. Statistically significant differences in protein expression on control versus CSE PBMC-derived sEVs detected by the MACSplex exosome kit were analyzed with two-way ANOVA, followed by Tukey's multiple comparisons test. Significance for tests was defined as $p < 0.05$.

Acknowledgements: We would like to thank Prof. Mandy Pefers at the University of Liverpool for her help with the proteomic analysis of EV samples.

Conflict of interest: The authors declare no commercial or financial conflict of interest.

Author contributions: N.G. designed and performed the experiments, analyzed data, and wrote the manuscript. Z.N. and K.A. carried out TEM and NTA analysis. V.J. revised the manuscript. D.O. supervised the experiments and revised the manuscript. L.F. conceived this research, supervised the experiments, and revised the manuscript.

Ethics declaration: All procedures of human samples were conducted under the approval of Ethics Committee of the University of Nottingham Medical School (FMHS REC ref 121–1706), and informed patient consent was obtained from all subjects in advanced of sample collection.

Funding statement: The ID7000C spectral cell analyzer was funded by the Biotechnology and Biological Sciences Research Council to L.F. and D.O. (BBSRC) (BB/T017619/1). The ImageStream X MKII was funded by the Wellcome to L.F. and D.O. (grant reference 212908/Z/18/Z) N.G. was supported by a University of Nottingham Vice Chancellor's International Research Scholarship.

Data availability statement: The data that support the findings of this study are available from the corresponding author upon reasonable request.

Peer review: The peer review history for this article is available at <https://publons.com/publon/10.1002/eji.202250143>

References

- Zhou, X., Xie, F., Wang, L., Zhang, L., Zhang, S., Fang, M. and Zhou, F., The function and clinical application of extracellular vesicles in innate immune regulation. *Cell. Mol. Immunol.* 2020. 17: 323–334.

- 2 Yáñez-Mó, M., Siljander, P. R. M., Andreu, Z., Bedina Zavec, A., Borrás, F. E., Buzas, E. I., Buzas, K. et al., Biological properties of extracellular vesicles and their physiological functions. *J. Extracell. Vesicles* 2015. 4: 27066.
- 3 Buzas, E. I., The roles of extracellular vesicles in the immune system. *Nat. Rev. Immunol.* 2022. 23: 236–250
- 4 Javeed, N. and Mukhopadhyay, D., Exosomes and their role in the micro-/macro-environment: a comprehensive review. *J. Biomed. Res.* 2017. 31: 386–394.
- 5 Ter-Ovanesyan, D., Norman, M., Lazarovits, R., Trieu, W., Lee, J. H., Church, G. M. and Walt, D. R., Framework for rapid comparison of extracellular vesicle isolation methods. *Elife.* 2021. 10: e70725.
- 6 Jankovičová, J., Sečová, P., Michalková, K. and Antalíková, J., Tetraspanins, more than markers of extracellular vesicles in reproduction. *Int. J. Mol. Sci.* 2020. 21: 7568.
- 7 Gutiérrez-Vázquez, C., Villarroja-Beltri, C., Mittelbrunn, M. and Sánchez-Madrid, F., Transfer of extracellular vesicles during immune cell-cell interactions. *Immunol. Rev.* 2013. 251: 125–142.
- 8 Yang, P., Peng, Y., Feng, Y., Xu, Z., Feng, P., Cao, J., Chen, Y. et al., Immune cell-derived extracellular vesicles—new strategies in cancer immunotherapy. *Front. Immunol.* 2021. 12: 771551.
- 9 Blanchard, N., Lankar, D., Faure, F., Regnault, A., Dumont, C., Raposo, G. and Hivroz, C., TCR activation of human T cells induces the production of exosomes bearing the TCR/CD3/zeta complex. *J. Immunol.* 2002. 168: 3235–3241.
- 10 Muntasell, A., Berger, A. C. and Roche, P. A., T cell-induced secretion of MHC class II-peptide complexes on B cell exosomes. *EMBO J.* 2007. 26: 4263–4272.
- 11 Raposo, G., Nijman, H. W., Stoorvogel, W., Liejendekker, R., Harding, C. V., Melief, C. J. and Geuze, H. J., B lymphocytes secrete antigen-presenting vesicles. *J. Exp. Med.* 1996. 183: 1161–1172.
- 12 Buschow, S. I., Balkom, B. W. M., Aalberts, M., Heck, A. J. R., Wauben, M. and Stoorvogel, W., MHC class II-associated proteins in B-cell exosomes and potential functional implications for exosome biogenesis. *Immunol. Cell Biol.* 2010. 88: 851–856.
- 13 Qazi, K. R., Gehrman, U., Domange Jordö, E., Karlsson, M. C. I. and Gabrielsson, S., Antigen-loaded exosomes alone induce Th1-type memory through a B-cell-dependent mechanism. *Blood.* 2009. 113: 2673–2683.
- 14 Hao, S., Yuan, J. and Xiang, J., Nonspecific CD4(+) T cells with uptake of antigen-specific dendritic cell-released exosomes stimulate antigen-specific CD8(+) CTL responses and long-term T cell memory. *J. Leukoc. Biol.* 2007. 82: 829–838.
- 15 Giri, P. K. and Schorey, J. S., Exosomes derived from M. Bovis BCG infected macrophages activate antigen-specific CD4+ and CD8+ T cells in vitro and in vivo. *PLoS One.* 2008. 3: e2461.
- 16 Skokos, D., Botros, H. G., Demeure, C., Morin, J., Peronet, R., Birkenmeier, G., Boudaly, S. et al., Mast cell-derived exosomes induce phenotypic and functional maturation of dendritic cells and elicit specific immune responses in vivo. *J. Immunol.* 2003. 170: 3037–3045.
- 17 Bhatnagar, S. and Schorey, J. S., Exosomes released from infected macrophages contain *Mycobacterium avium* glycopeptidolipids and are proinflammatory. *J. Biol. Chem.* 2007. 282: 25779–25789.
- 18 Hedlund, M., Nagaeva, O., Kargl, D., Baranov, V. and Mincheva-Nilsson, L., Thermal- and oxidative stress causes enhanced release of NKG2D ligand-bearing immunosuppressive exosomes in leukemia/lymphoma T and B cells. *PLoS One.* 2011. 6: e16899.
- 19 Monleón, I., Martínez-Lorenzo, M. J., Monteagudo, L., Lasierra, P., Taulés, M., Iturralde, M., Piñeiro, A. et al., Differential secretion of Fas ligand- or APO2 ligand/TNF-related apoptosis-inducing ligand-carrying microvesicles during activation-induced death of human T cells. *J. Immunol.* 2001. 167: 6736–6744.
- 20 Xie, Y., Zhang, H., Li, W., Deng, Y., Munegowda, M. A., Chibbar, R., Qureshi, M. et al., Dendritic cells recruit T cell exosomes via exosomal LFA-1 leading to inhibition of CD8+ CTL responses through downregulation of peptide/MHC class I and Fas ligand-mediated cytotoxicity. *J. Immunol.* 2010. 185: 5268–5278.
- 21 Kadota, T., Fujita, Yu, Yoshioka, Y., Araya, J., Kuwano, K. and Ochiya, T., Extracellular vesicles in chronic obstructive pulmonary disease. *Int. J. Mol. Sci.* 2016. 17: 1801.
- 22 Wahlund, C. J. E., Eklund, A., Grunewald, J. and Gabrielsson, S., Pulmonary extracellular vesicles as mediators of local and systemic inflammation. *Front. Cell Dev. Biol.* 2017. 5: 39.
- 23 Bazzan, E., Radu, C. M., Tinè, M., Neri, T., Biondini, D., Semenzato, U., Casara, A. et al., Microvesicles in bronchoalveolar lavage as a potential biomarker of COPD. *Am. J. Physiol. Lung Cell. Mol. Physiol.* 2021. 320: L241–L245.
- 24 Rodriguez, M., Silva, J., López-Alfonso, A., López-Muñoz, M. B., Peña, C., Domínguez, G., García, J. M. et al., Different exosome cargo from plasma/bronchoalveolar lavage in non-small-cell lung cancer. *Genes, Chromosomes & Cancer* 2014. 53: 713–724.
- 25 Fujita, Y., Kosaka, N., Araya, J., Kuwano, K. and Ochiya, T., Extracellular vesicles in lung microenvironment and pathogenesis. *Trends Mol. Med.* 2015. 21: 533–542.
- 26 Gomez, N., James, V., Onion, D. and Fairclough, L. C., Extracellular vesicles and chronic obstructive pulmonary disease (COPD): a systematic review. *Respir. Res.* 2022. 23: 82.
- 27 Qiu, Q., Dan, X., Yang, C., Hardy, P., Yang, Z., Liu, G. and Xiong, W., Increased airway T lymphocyte microparticles in chronic obstructive pulmonary disease induces airway epithelial injury. *Life Sci.* 2020. 261: 118357.
- 28 Genschmer, K. R., Russell, D. W., Lal, C., Szul, T., Bratcher, P. E., Noerager, B. D., Abdul Roda, M. et al., Activated PMN exosomes: pathogenic entities causing matrix destruction and disease in the lung. *Cell* 2019. 176: 113–126.
- 29 Margaroli, C., Madison, M. C., Viera, L., Russell, D. W., Gaggari, A., Genschmer, K. R. and Blalock, J. E., A novel in vivo model for extracellular vesicle-induced emphysema. *JCI Insight.* 2022. 7: e153560
- 30 Zappasodi, R., Budhu, S., Abu-Akeel, M. and Merghoub, T., In vitro assays for effector T cell functions and activity of immunomodulatory antibodies. *Methods Enzymol.* 2020. 631: 43–59.
- 31 Théry, C., Witwer, K. W., Aikawa, E., Alcaraz, M. J., Anderson, J. D., Andriantsitohaina, R., Antoniou, A. et al., Minimal information for studies of extracellular vesicles 2018 (MISEV2018): a position statement of the International Society for Extracellular Vesicles and update of the MISEV2014 guidelines. *J. Extracell. Vesicles* 2018. 7: 1535750.
- 32 Welsh, J. A., Van Der Pol, E., Arkesteijn, G. J. A., Bremer, M., Brisson, A., Coumans, F., Dignat-George, F. et al., MIFlowCyt-EV: a framework for standardized reporting of extracellular vesicle flow cytometry experiments. *J. Extracell. Vesicles* 2020. 9: 1713526.
- 33 Gray, W. D., Mitchell, A. J. and Searles, C. D., An accurate, precise method for general labeling of extracellular vesicles. *MethodsX* 2015. 2: 360–367.
- 34 Luo, T., Chen, S. Y., Qiu, Z. X., Miao, Y. R., Ding, Y., Pan, X. Y., Li, Y. et al., Transcriptomic features in a single extracellular vesicle via single-cell RNA sequencing. *Small Methods* 2022: 2200881.
- 35 Cismasiu, V. B. and Popescu, L. M., Telocytes transfer extracellular vesicles loaded with microRNAs to stem cells. *J. Cell. Mol. Med.* 2015. 19: 351–358.

- 36 Nizamudeen, Z. A., Xerri, R., Parmenter, C., Suain, K., Markus, R., Chakrabarti, L. and Sottile, V., Low-power sonication can alter extracellular vesicle size and properties. *Cells*. 2021. 10: 2413.
- 37 Alkhattabi, N., Todd, I., Negm, O., Tighe, P. J. and Fairclough, L. C., Tobacco smoke and nicotine suppress expression of activating signaling molecules in human dendritic cells. *Toxicol. Lett.* 2018. 299: 40–46.
- 38 Aoshiba, K., Tamaoki, J. and Nagai, A., Acute cigarette smoke exposure induces apoptosis of alveolar macrophages. *Am. J. Physiol. Lung Cell. Mol. Physiol.* 2001. 281: L1392–L1401.
- 39 Mian, M. F., Lauzon, N. M., Stämpfli, M. R., Mossman, K. L. and Ashkar, A. A., Impairment of human NK cell cytotoxic activity and cytokine release by cigarette smoke. *J. Leukoc. Biol.* 2008. 83: 774–784.
- 40 Su, Y., Cao, W., Han, Z. and Block, E. R., Cigarette smoke extract inhibits angiogenesis of pulmonary artery endothelial cells: the role of calpain. *Am. J. Physiol. Lung Cell. Mol. Physiol.* 2004. 287: L794–L800.
- 41 Wongtrakool, C., Grooms, K., Bijli, K. M., Crothers, K., Fitzpatrick, A. M. and Hart, C. M., Nicotine stimulates nerve growth factor in lung fibroblasts through an NFkappaB-dependent mechanism. *PLoS One*. 2014. 9: e109602.
- 42 Matthiesen, R., Gameiro, P., Henriques, A., Bodo, C., Moraes, M. C. S., Costa-Silva, B., Cabeçadas, J. et al., Extracellular vesicles in diffuse large B cell lymphoma: characterization and diagnostic potential. *Int. J. Mol. Sci.* 2022. 23: 13327.
- 43 Pienimaeki-Roemer, A., Kuhlmann, K., Böttcher, A., Konovalova, T., Black, A., Orsó, E., Liebisch, G. et al., Lipidomic and proteomic characterization of platelet extracellular vesicle subfractions from senescent platelets. *Transfusion* 2015. 55: 507–521.
- 44 Rosa-Fernandes, L., Rocha, V. B., Carregari, V. C., Urbani, A. and Palmisano, G., A perspective on extracellular vesicles proteomics. *Front. Chem.* 2017. 5: 102.
- 45 Lübke, T., Lobel, P. and Sleat, D. E., Proteomics of the lysosome. *Biochim. Biophys. Acta* 2009. 1793: 625–635.
- 46 Saleem, R. A., Smith, J. J. and Aitchison, J. D., Proteomics of the peroxisome. *Biochim. Biophys. Acta* 2006. 1763: 1541–1551.
- 47 Lannigan, J. and Erdbrugger, U., Imaging flow cytometry for the characterization of extracellular vesicles. *Methods (San Diego, Calif.)* 2017. 112: 55–67.
- 48 De Rond, L., Van Der Pol, E., Hau, C. M., Varga, Z., Sturk, A., Van Leeuwen, T. G., Nieuwland, R. et al., Comparison of generic fluorescent markers for detection of extracellular vesicles by flow cytometry. *Clin. Chem.* 2018. 64: 680–689.
- 49 Mathieu, M., Névo, N., Jouve, M., Valenzuela, J. I., Maurin, M., Verweij, F. J., Palmulli, R. et al., Specificities of exosome versus small ectosome secretion revealed by live intracellular tracking of CD63 and CD9. *Nat. Commun.* 2021. 12: 4389.
- 50 Barranco, I., Padilla, L., Parrilla, I., Álvarez-Barrientos, A., Pérez-Patiño, C., Peña, F. J., Martínez, E. A. et al., Extracellular vesicles isolated from porcine seminal plasma exhibit different tetraspanin expression profiles. *Sci. Rep.* 2019. 9: 11584.
- 51 Ibrahim, S., Hedia, M., Taqi, M. O., Derbala, M. K., Mahmoud, K. G. M., Ahmed, Y., Sosa, A. S. et al., Extracellular vesicles in low volume uterine lavage and serum: novel and promising biomarker for endometritis in Arabian mares. *BMC Vet. Res.* 2022. 18: 42.
- 52 Han, C., Kang, H., Yi, J., Kang, M., Lee, H., Kwon, Y., Jung, J. et al., Single-vesicle imaging and co-localization analysis for tetraspanin profiling of individual extracellular vesicles. *J. Extracell. Vesicles* 2021. 10: e12047.
- 53 Karimi, N., Dalirfardouei, R., Dias, T., Lötvall, J. and Lässer, C., Tetraspanins distinguish separate extracellular vesicle subpopulations in human serum and plasma - Contributions of platelet extracellular vesicles in plasma samples. *J. Extracell. Vesicles* 2022. 11: e12213.
- 54 Andreu, Z. and Yáñez-Mó, M. A., Tetraspanins in extracellular vesicle formation and function. *Front. Immunol.* 2014. 5: 442.
- 55 d'Alessandro, M., Soccio, P., Bergantini, L., Cameli, P., Scioscia, G., Foschino Barbaro, M. P., Lacedonia, D. et al., Extracellular vesicle surface signatures in IPF patients: a multiplex bead-based flow cytometry approach. *Cells*, 2021. 10: 1045.
- 56 Puhm, F., Boilard, E. and Machlus, K. R., Platelet extracellular vesicles: beyond the blood. *Arterioscler. Thromb. Vasc. Biol.* 2021. 41: 87–96.
- 57 Tao, S. C., Guo, S. C. and Zhang, C. Q., Platelet-derived extracellular vesicles: an emerging therapeutic approach. *Int. J. Biol. Sci.* 2017. 13: 828–834.
- 58 Bernhard, D., Huck, C. W., Jakschitz, T., Pfister, G., Henderson, B., Bonn, G. K. and Wick, G., Development and evaluation of an in vitro model for the analysis of cigarette smoke effects on cultured cells and tissues. *J. Pharmacol. Toxicol. Methods* 2004. 50: 45–51.
- 59 Russell, A. E., Liao, Z., Tkach, M., Tarwater, P. M., Ostrowski, M., Théry, C., Witwer, K. W., Cigarette smoke-induced extracellular vesicles from dendritic cells alter T-cell activation and HIV replication. *Toxicol. Lett.* 2022. 360: 33–43.
- 60 Pugholm, L. H., Bæk, R., Søndergaard, E. K. L., Revenfeld, A. L. S., Jørgensen, M. M. and Varming, K., Phenotyping of leukocytes and leukocyte-derived extracellular vesicles. *J Immunol Res.* 2016. 2016: 6391264.
- 61 Veerman, R. E., Güçlüler Akpınar, G., Eldh, M. and Gabrielsson, S., Immune cell-derived extracellular vesicles – functions and therapeutic applications. *Trends Mol. Med.* 2019. 25: 382–394.
- 62 Elgueta, R., Benson, M. J., De Vries, V. C., Wasiuk, A., Guo, Y. and Noelle, R. J., Molecular mechanism and function of CD40/CD40L engagement in the immune system. *Immunol. Rev.* 2009. 229: 152–172.
- 63 Chatzigeorgiou, A., Lyberi, M., Chatzilymperis, G., Nezos, A. and Kamper, E., CD40/CD40L signaling and its implication in health and disease. *Biofactors*. 2009. 35: 474–483.
- 64 Laman, J. D., Claassen, E. and Noelle, R. J., Functions of CD40 and Its Ligand, gp39 (CD40L). *Crit. Rev. Immunol.* 2017. 37: 371–420.
- 65 Román-Fernández, I. V., García-Chagollán, M., Cerpa-Cruz, S., Jave-Suárez, L. F., Palafox-Sánchez, C. A., García-Arellano, S., Sánchez-Zuno, G. A. et al., Assessment of CD40 and CD40L expression in rheumatoid arthritis patients, association with clinical features and DAS28. *Clin. Exp. Med.* 2019. 19: 427–437.
- 66 Jabara, H. H., Fu, S. M., Geha, R. S. and Vercelli, D., CD40 and IgE: synergism between anti-CD40 monoclonal antibody and interleukin 4 in the induction of IgE synthesis by highly purified human B cells. *J. Exp. Med.* 1990. 172: 1861–1864.
- 67 Liang, Y., Shen, Y., Kuang, L., Zhou, G., Zhang, L., Zhong, X., Zhang, J. et al., Cigarette smoke exposure promotes differentiation of CD4(+) T cells toward Th17 cells by CD40-CD40L costimulatory pathway in mice. *Int J Chron Obstruct Pulmon Dis.* 2018. 13: 959–968.
- 68 Givi, M. E., Folkerts, G., Wagenaar, G. T. M., Redegeld, F. A. and Mortaz, E., Cigarette smoke differentially modulates dendritic cell maturation and function in time. *Respir. Res.* 2015. 16: 131.
- 69 Aatonen, M. T., Öhman, T., Nyman, T. A., Laitinen, S., Grönholm, M. and Siljander, P. R. M., Isolation and characterization of platelet-derived extracellular vesicles. *J. Extracell. Vesicles* 2014. 3: 24692
- 70 O'shea, D., Cawood, T. J., O'farrelly, C. and Lynch, L., Natural killer cells in obesity: impaired function and increased susceptibility to the effects of cigarette smoke. *PLoS One* 2010. 5: e8660.
- 71 Mian, M. F., Pek, E. A., Mossman, K. L., Stämpfli, M. R. and Ashkar, A. A., Exposure to cigarette smoke suppresses IL-15 generation and its regulatory NK cell functions in poly I:C-augmented human PBMCs. *Mol. Immunol.* 2009. 46: 3108–3116.

- 72 Roos-Engstrand, E., Pourazar, J., Behndig, A. F., Blomberg, A. and Bucht, A., Cytotoxic T cells expressing the co-stimulatory receptor NKG2 D are increased in cigarette smoking and COPD. *Respir. Res.* 2010. 11: 128.
- 73 Piali, L., Hammel, P., Uherek, C., Bachmann, F., Gisler, R. H., Dunon, D. and Imhof, B. A., CD31/PECAM-1 is a ligand for alpha v beta 3 integrin involved in adhesion of leukocytes to endothelium. *J. Cell Biol.* 1995. 130: 451–460.
- 74 Liu, L. and Shi, G. P., CD31: beyond a marker for endothelial cells. *Cardiovasc. Res.* 2012. 94: 3–5.
- 75 Marelli-Berg, F. M., Clement, M., Mauro, C. and Caligiuri, G., An immunologist's guide to CD31 function in T-cells. *J. Cell Sci.* 2013. 126(Pt): 2343–2352.
- 76 Liu, H., Ding, L., Zhang, Y. and Ni, S., Circulating endothelial microparticles involved in lung function decline in a rat exposed in cigarette smoke maybe from apoptotic pulmonary capillary endothelial cells. *J. Thorac. Dis.* 2014. 6: 649–655.
- 77 Hodge, S., Matthews, G., Mukaro, V., Ahern, J., Shivam, A., Hodge, G., Holmes, M. et al., Cigarette smoke-induced changes to alveolar macrophage phenotype and function are improved by treatment with procysteine. *Am. J. Respir. Cell Mol. Biol.* 2011. 44: 673–681.
- 78 Wiczorek, M., Abualrous, E. T., Sticht, J., Álvaro-Benito, M., Stolzenberg, S., Noé, F. and Freund, C., Major histocompatibility complex (MHC) class I and MHC class II proteins: conformational plasticity in antigen presentation. *Front. Immunol.* 2017. 8: 292.
- 79 Boyne, C., Lennox, D., Beech, O., Powis, S. J. and Kumar, P., What is the role of HLA-I on cancer derived extracellular vesicles? Defining the challenges in characterisation and potential uses of this ligandome. *Int. J. Mol. Sci.* 2021. 22: 13554.
- 80 Ryu, A. R., Kim, D. H., Kim, E. and Lee, M. Y., The potential roles of extracellular vesicles in cigarette smoke-associated diseases. *Oxid. Med. Cell Longev.* 2018. 2018: 4692081.
- 81 Wu, F., Yin, Z., Yang, L., Fan, J., Xu, J., Jin, Y., Yu, J. et al., Smoking induced extracellular vesicles release and their distinct properties in non-small cell lung cancer. *J. Cancer.* 2019. 10: 3435–3443.

Abbreviations: COPD: chronic obstructive pulmonary disease · CSE: cigarette smoke extract · EVs: extracellular vesicles · HLA: human leukocyte antigen · IFC: imaging flow cytometry · MISEV: Minimal Information for Studies of Extracellular Vesicles · NTA: nanoparticle tracking analysis · sEVs: small EVs · TEM: transmission electron microscopy

Full correspondence: Prof. Lucy C. Fairclough, School of Life Sciences, The University of Nottingham, Life Sciences Building, Nottingham NG7 2RD, UK
e-mail: lucy.fairclough@nottingham.ac.uk

Received: 23/8/2022
Revised: 24/2/2023
Accepted: 14/3/2023
Accepted article online: 16/3/2023